Simultaneous competition and coexistence between charge-density waves and reentrant superconductivity in the pressure-temperature phase diagram of the molecular conductor TTF $[Ni(dmit)_2]_2$ (where TTF is tetrathiafulvalene and dmit is the 1,3-dithia-2-thione-4,5-dithiolato group)

L. Brossard and M. Ribault
Laboratoire de Physique des Solides, Bâtiment 510, Université Paris—Sud, 91405 Orsay, France

L. Valade and P. Cassoux
Laboratoire de Chimie de Coordination du Centre National de la Recherche Scientifique, 205 route de Narbonne, 31077 Toulouse CEDEX, France

(Received 29 January 1990; revised manuscript received 16 April 1990)

The pressure-temperature phase diagram of the quasi-one-dimensional molecular superconductor TTF $[Ni(dmit)_2]_2$ has been carefully determined by ac resistivity measurements up to 14 kbar. Increasing pressures induce electronic phase transitions between a high-temperature metal and successive, metallic or semimetallic, semiconducting and reentrant superconducting ground states. This unusual phase diagram is compared with that of TTF $[Pd(dmit)_2]_2$. It is discussed in connection with ambient-pressure charge-density-wave (CDW) instabilities, the wave vector of which can be well accounted for by an original conduction-band structure involving both the highest occupied molecular orbitals and the lowest unoccupied molecular orbitals of the acceptor slabs. It is confirmed that the superconducting temperature increases slowly with increasing pressure. It is suggested that the superconductivity coexists with a high-temperature CDW instability and is in weak competition with low-temperature CDW fluctuations; these CDW's affect different parts of the Fermi surface.

INTRODUCTION

The interplay between competing instabilities inside an electronic gas of low dimensionality is a topic of increasing interest. Contrary to Mott insulators[1] in which the electrons are held in localized states by correlation energy arising either from Coulomb interaction between electrons or from strong interactions with neighboring ions, several mechanisms may be responsible for the "metal-semiconductor" transition in ordered structures, i.e., in the absence of Anderson localization.[2] These mechanisms are known to result from instabilities of the electron-hole spectrum in some areas of the Fermi surface (FS) against the electron-phonon and the electron-electron exchange interactions: the relative strength of these interactions[3] determines the nature of these instabilities, either charge-density waves (CDW's) associated with periodic lattice distortions (PLD's),[4] or spin-density waves (SDW's),[5] respectively. However, their occurrence is connected with the anisotropy of the FS:[6] they occur only for some characteristic wave vector **q** for which the susceptibility of the electron gas becomes large. This can be achieved through a progressive nesting of relatively large electron and hole areas of the FS, leading to a temperature-gap opening: this happens in the CDW-Peierls distortion encountered in $K_2[Pt(CN)_4]Br_{0.3}3H_2O$ (KCP),[7] TTF-7,7,8,8-tetracyanoquinodimethane,[8] 1*T*-TaS_2 and -$TaSe_2$ (octahedral coordination),[9] as well as in the SDW ground state of many organic conductors.[10] This can also be achieved through saddle points located very close to the Fermi level,[11] the so-called Van Hove singularities for which only a minor fraction of diffuse states of the FS is removed, leading to metal-semimetal or metal-metal transitions: this is observed in the CDW ground states of 2*H*-TaS_2, -$TaSe_2$, and -$NbSe_2$ (trigonal prismatic coordination),[12] $NbSe_3$,[13] and accounts also for the martensitic transition in *A*15 compounds.[14]

These electron-hole instabilities may in turn become unstable versus interactions involving attraction between electrons, either by varying the temperature or the pressure or by alloying. A superconducting ground state may be in close competition either with SDW (case of the Bechgaard and related salts[15]) or with CDW [case of the 2*H*-dichalcogenides[16] and $NbSe_3$ (Ref. 13)] instabilities. Moreover, the superconducting temperature T_c generally decreases with increasing pressure in a well condensed superconducting regime, except in the 2*H*-dichalcogenides[16] and *A*15 compounds.[17]

The recently synthetized one-dimensional (1D) TTF-$[M(dmit)_2]_2$ conductors,[18] with M=Ni, Pd are multi-parallel-band systems,[19] and their interest is multiplied in light of the following points:

(i) X-ray diffuse scattering studies at ambient pressure reveal many sets of 1D structural fluctuations[20] associated with CDW instabilities, which take place along the *b* stacking axis of the *C*2/*c* monoclinic structure.

(ii) The reduced wave vectors **q** of these successive structural instabilities are well assigned with the intersection between the Fermi level and the bunches of the bands built on both the highest occupied molecular orbit-

al (HOMO) and lowest unoccupied molecular orbital (LUMO) of the acceptors $M(\text{dmit})_2$ slabs only.[21] This accounts for the intricate 1D multi-parallel-band structure, where the LUMO of the acceptors overlap not only the HOMO of the TTF as usual, but also those of the acceptors.[21]

(iii) While the CDW's in the Pd compound are associated with the high-temperature metal-semiconductor transition,[22] the Ni counterpart remains metallic down to very low temperature, and its magnetoresistive properties at 4.2 K reveal a departure from 1D behavior.[23]

(iv) The pressure-temperature (P,T) phase diagram of the Pd salt is characterized[22] by a strong competition over a 4-kbar interval between the low-pressure CDW and high-pressure superconducting ground states, instead of the usual SDW-superconducting competition observed in the Bechgaard salts.[15]

(v) The Ni salt is superconducting under pressure,[24] but contrary to its Pd counterpart, T_c increases slowly with increasing pressure,[25] which is reminiscent of the $2H$-chalcogenides and $A15$ behavior.

Hence, the aim of this work is to present the detailed (P,T) phase diagram of the TTF $[\text{Ni(dmit)}_2]_2$ salt. A preliminary sketch of this diagram has already been published.[26] First, pressure-dependent conductivity measurements at 300 K are presented. Then, new temperature-dependent resistivity results at ambient pressure are presented and compared with other measurements. Next, the temperature dependence of the resistivity under pressure is reported. Finally, the successive phase transitions between (semi) metallic, semiconducting, and reentrant superconducting ground states induced by pressure are detailed in the complete phase diagram of TTF $[\text{Ni(dmit)}_2]_2$. A tentative discussion of these results may be derived from band structure calculations[21] and from a comparison with the phase diagram of the analog TTF $[\text{Pd(dmit)}_2]_2$ salt.[22] These calculations predict a removal under pressure of the 2D character of the zone center of the Ni salt. In their present state, our results suggest a coexistence of a high-temperature CDW instability and a weak competition of low-temperature CDW fluctuations, with a reentrant superconducting ground state above 5.5 kbar.

EXPERIMENTAL DETAILS

Samples

Black shiny needles of TTF $[\text{Ni(dmit)}_2]_2$ were prepared[18] by slow interdiffusion of saturated solutions of $(\text{TTF})_3(\text{BF}_4)_2$ and $(n\text{-Bu}_4\text{N})[\text{Ni(dmit)}_2]$. Ambient-pressure x-ray-diffraction measurements at 300 and 100 K lead to the C-centered monoclinic structure whose stereoscopic view along the b stacking axis is shown in Fig. 1. Individual units of TTF alternate with slabs of Ni(dmit)_2 along the a axis in the a-c plane. The spacing between stack sites is $b = 3.73$ Å, but due to different tilted orientations, the interplanar spacing is 3.55 Å within the Ni(dmit)_2 stack and 3.65 Å within the TTF one.[27] These spacings are significantly larger than in the Pd derivative, despite the shrinkage expected from atomic radius considerations. As already pointed out in Ref. 22, this ensures weaker intermolecular intrastack S-S overlap and hence a weaker 1D character than in the Pd salt case, while the interactions in the ac plane remain similar.

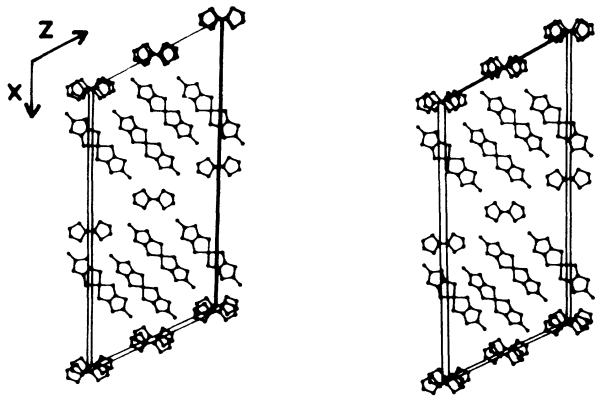

FIG. 1. Stereoscopic view along the stacking b axis of the centered monoclinic unit cell of TTF $[M(\text{dmit})_2]_2$ with M=Ni, Pd.

The phase diagram is derived from ac low-frequency longitudinal resistivity measurements performed via the standard four-point method, at 23 different pressures up to 14 kbar, and upon 15 samples. They were brought out either from the same batch as the so-called "M" sample—which was studied in 1986 (Ref. 24)—or from different batches which were prepared approximately at the same time. Since that time they were kept under vacuum and sheltered from the light.

Experimental

Annealed gold wires (cross-sectional diameter of 17 μm) first soldered on the copper feedthroughs of the Cu:Be obturator were then carefully pasted with silver paint on annular gold patches which were evaporated on the samples ($4\times0.05\times0.015$ mm^3). The pasting process was carried out using a micromanipulator. The contact resistances were better than 10% of the sample resistance. The obturator was fitted into a Teflon cell filled with a fluid used as pressure transmitting and sample thermalizing medium. This fluid was octane for the experiments performed at 250 and 500 bars, and isopentane for the measurements on the "M" sample carried out first at 7 kbar (Ref. 24) and then at 4 kbar (measurements called $M1$ and $M2$, respectively). For all the other pressures, the fluid was a mixture of alcanes in order to expand its freezing temperature range and hence reduce the damage of the contact resistances as well as the induced strains on the samples during the freezing process. This was done in order to perform as many measurements as possible at different pressures on the same sample. Similar care was taken in all cases to ensure a very slow cooling and heating process (6 K/h). These procedures have been quite successful since two or three reliable measurements at different pressures were obtained with several samples by using this alcane mixture instead of a pure alcane. The resistivity curves show no jumps and the su-

perconducting transition widths (0.2 to 0.3 K) are notably narrower than when using isopentane alone [0.6 K (Ref. 24)]. However, despite these improvements, the pressures obtained at low temperature are not so hydrostatic as one may obtain with He gas technique.[28] This may originate in the broad superconducting and insulating entrances experimentally observed in a very narrow pressure range (200 bars) around 5.4 kbar.

Since the pressure bomb is a clamp one, it is crucial to measure the pressure at low temperature. With this in mind, a heavily doped *InSb*:Te manometer[29] was mounted close to the sample in order to monitor the pressure at 300 K and during the cooling: the loss of pressure between 300 and 150 K range from 2.5 to 4 kbar at high and low pressure, respectively. The temperature dependence of the manometer resistivity is small compared to its pressure dependence and also pressure independent.[29] Moreover, all the pressures were determined in a reproducible way with the same manometer. Hence, the low-temperature pressures were measured with an accuracy better than 80 bars at low pressure and 50 bars around 10 kbar, respectively. This also ensures a good reliability in the relative scale of our pressure measurements. The clamp *Cu*:Be vessel was fixed at the bottom of the mixing chamber of a dilution refrigerator. The temperature was measured with Pt and Ge thermometers above and below 40 K, respectively. The samples were measured with constant current, at 100 and 10 μA in the metallic and activated regimes, respectively. Care was taken to avoid Joule heating of the sample in the case of either damaged current contact resistance or a too high sample resistance.

RESULTS AND ANALYSIS

Pressure dependent conductivity at 300 K

As shown in Fig. 2, the room-temperature conductivities σ of the Ni and Pd salts increase linearly with pressure up to about 4 and 13 kbar, respectively. The initial relative slope $d\sigma/\sigma_0 dP$ for the Ni salt is 3 times larger than for its Pd counterpart (0.11/kbar). The actual Ni salt value (0.33/kbar) is slightly different from the previously published one[22] but results from more accurate measurements. At 5.3 kbar, the conductivity of the Ni salt catches up that of the Pd salt at ambient pressure, and its relative slope becomes equal to that of the Pd salt. These different behaviors reflect the larger compressibility or the smaller stiffness of the Ni salt lattice, which is in agreement with the already mentioned[22,27] shrinking of the Pd salt unit cell along the b axis at ambient pressure. At high pressure, the Ni salt conductivity shows a tendency to saturation, contrary to its Pd derivative.

Temperature-dependent resistivity at ambient pressure

X-ray diffuse scattering studies performed on single crystals of the Ni salt down to about 20 K (Ref. 20) have revealed one main 1D diffuse line at $q_1 = 0.40b^*$, which drives a structural transition at ca. 40 K. Such a result was quite surprising since this compound was known to stay metallic down to very low temperatures. In fact a log-log plot of the resistivity ρ versus T (Fig. 3) shows only a very weak departure from the $T^{1.65}$ power law between ~ 90 and 25 K. Similar T^n power laws are observed on other samples, n decreasing with the residual resistive ratio $\mathcal{R} = R(300\text{ K})/R(4\text{ K})$. The q_1 CDW instability can be related with the bunch of LUMO bands of the acceptor slabs (Fig. 4). This assignment is in agreement with thermopower data[30] showing that holes become the dominant carriers below 70 K. At lower temperature, the resistivity of the Ni compound shows (Fig. 3 and inset of Fig. 5) a more pronounced but still weak anomaly below 10 K, followed by a weak resistivity minimum at 1.5 K, or 3 K,[23] depending on the samples.

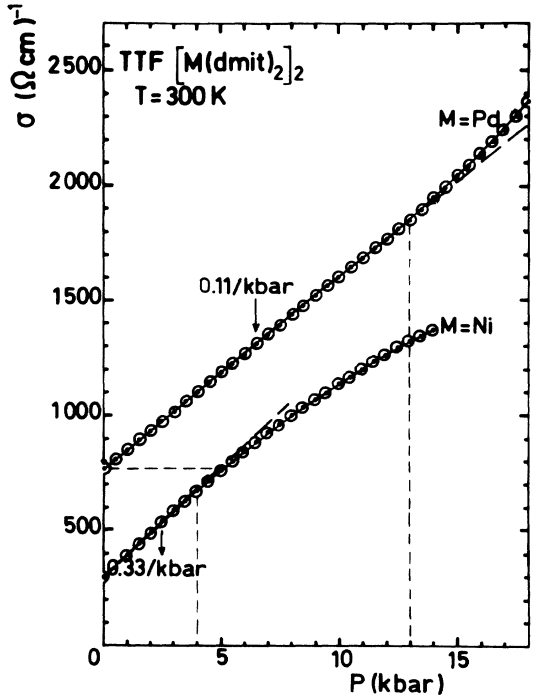

FIG. 2. Compared pressure dependence of the conductivities of TTF $[M(\text{dmit})_2]_2$ with M=Ni, Pd at 300 K.

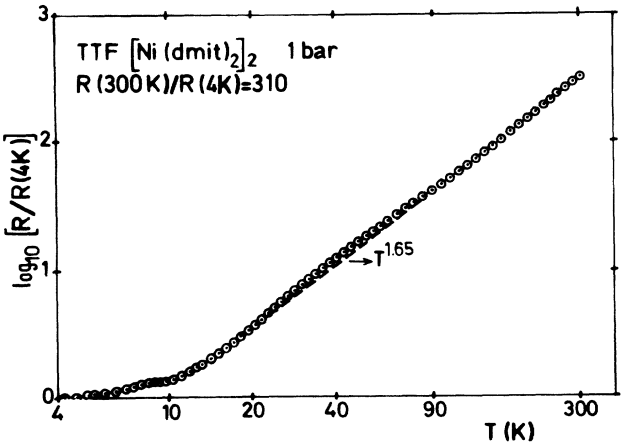

FIG. 3. High-temperature variation of the TTF $[Ni(dmit)_2]_2$ resistivity at ambient pressure in a log-log scale.

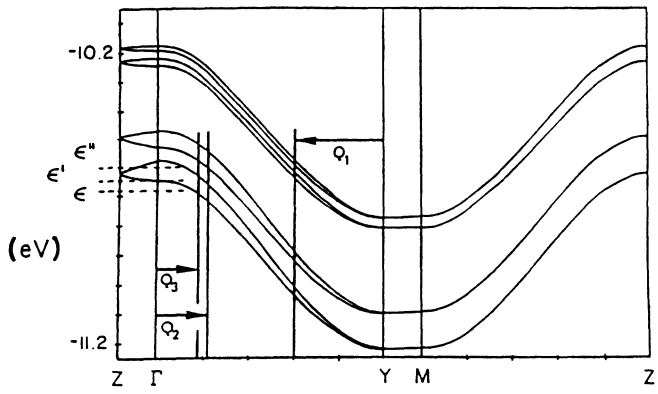

FIG. 4. Ambient-pressure band structure of $Ni(dmit)_2$ slabs of TTF $[Ni(dmit)_2]_2$ from Ref. 31: half the 1D critical wave vectors ($Q_i = \mathbf{q}_i/2$) measured by X-ray diffuse scattering (Ref. 20) are shown; ε, ε', and ε'' correspond to charge transfer equal to 0, 0.5, and 1, respectively.

This 10-K anomaly is observed only on samples characterized by a high $\mathcal{R}$ ratio, which could explain why it escaped detection in the past. Two other weaker 1D diffuse scatterings at $\mathbf{q}_2 = 0.22b^*$ and $\mathbf{q}_3 = 0.18b^*$ were detected later on.[31] When considering some electronic reorganization after the $\mathbf{q}_1$ condensation, these scatterings could be associated with $2k_F$ CDW instabilities within the bunch of the highest HOMO bands of the acceptors (Fig. 4). Thus, the weak 10-K resistivity bump and the increase of the resistivity below 1.5 K could result from the condensation of the $\mathbf{q}_2$ and $\mathbf{q}_3$ instabilities. Although a band approach neglects the low-temperature electron correlations including the Coulomb interactions between the condensed CDW's,[32] it is worthwhile to discuss the consequences of these preceding experiments upon the band structure and to compare them with other measurements. From the structural data, the charge transfer can be estimated at ~ 0.75 hole per TTF, leading to a Fermi level comprised between ε' and ε'' in Fig. 4. Hence, the only remaining carriers at temperatures well below 10 K come from the following:

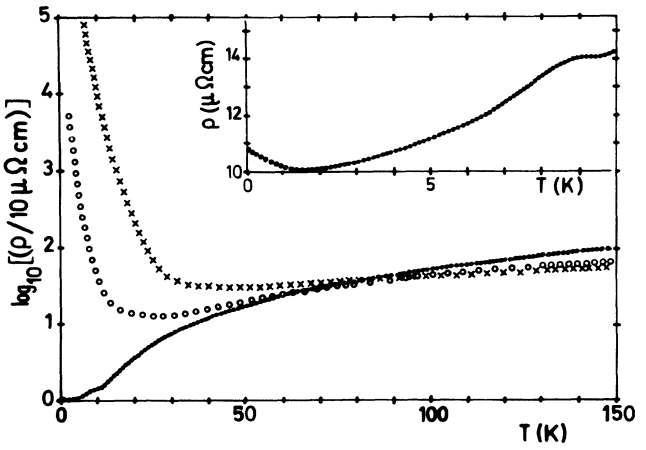

FIG. 5. log of the TTF $[Ni(dmit)_2]_2$ resistivity vs T at ambient pressure (· · · ·), 250 bars (○), and 500 bars (×); the inset shows the resistivity ρ below 10 K at ambient pressure.

(i) The TTF band (not shown in Fig. 4), in agreement with powder ^1H NMR measurements which not only show the 1D character of the TTF stacks, but do not reveal any gap opening in their electronic excitations down to 1.5 K.[33] Thus the origin of the increasing resistivity below 1.5 K could also result from such an instability on the TTF, although not exclusively.

(ii) The last partly occupied HOMO band of the acceptors, which shows an obvious 2D character at the center of the Brillouin zone (see Fig. 4 around the Γ point). This accounts for the departure from 1D behavior of the magnetoresistance at 4.2 K.[23] The absence of Shubnikov–de Haas oscillations could be explained by a too high Dingle temperature.

Temperature-dependent resistivity under pressure

The first effect of the pressure in the initial 500 bars is to induce a sharp resistivity increase observed below a T_{min} temperature where the resistivity is minimum (Fig. 5). T_{min} increases from 1.5 K at ambient pressure to 48 K at 500 bars. At higher pressure (Fig. 6), T_{min} first decreases to 23 K at 1 kbar and then varies up and down in a queer fashion up to 4 kbar. Above this pressure, T_{min} decreases exponentially with pressure following $d\ln(T_{min})/dP = -11.3\times10^{-2}$/kbar, which is 3 times the Pd salt corresponding value (-3.9×10^{-2}/kbar).[34]

Above T_{min}, the resistivity ρ shows some weak anomalies (Fig. 6): a first bump appears between 50 and 100 K whatever the pressure. A second bump appears below 35 K, when T_{min} is not too high (excepted at 1 kbar, where the bump is clearly visible below T_{min}). It is important to note that this bump disappears above 5.5 kbar. Both bumps are affected (Fig. 7) by an increasing current density (1.3 and 2.6 A/mm^2 corresponding to 530 and 1060 μA at 5.5 kbar). This is not the case of the resistivity minimum.

Below T_{min}, three pressure ranges are to be considered.

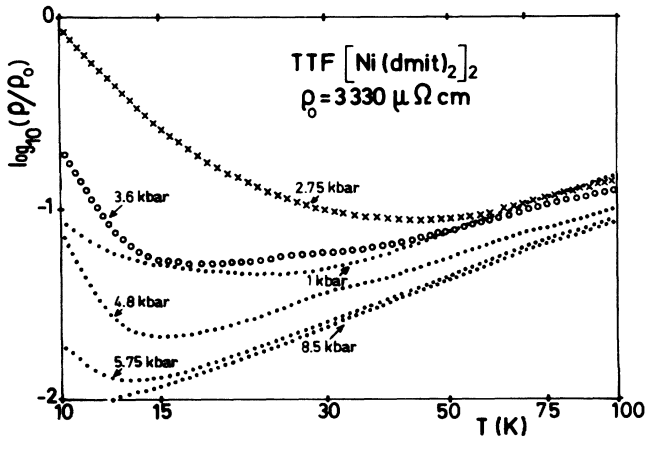

FIG. 6. log of the TTF $[Ni(dmit)_2]_2$ resistivity relative to ρ_0 (at 300 K and at ambient pressure) vs T: when the temperature T_{min} of the resistivity minimum is not too high, a small resistivity bump can be seen between T_{min} and a higher-temperature weak anomaly centered around 75 K.

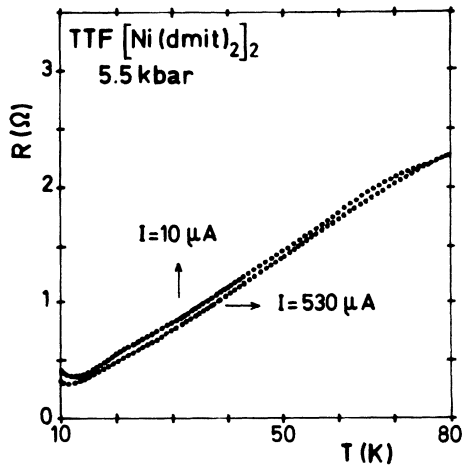

FIG. 7. Nonlinear effects on the resistance of TTF $[Ni(dmit)_2]_2$ at 5.5 kbar.

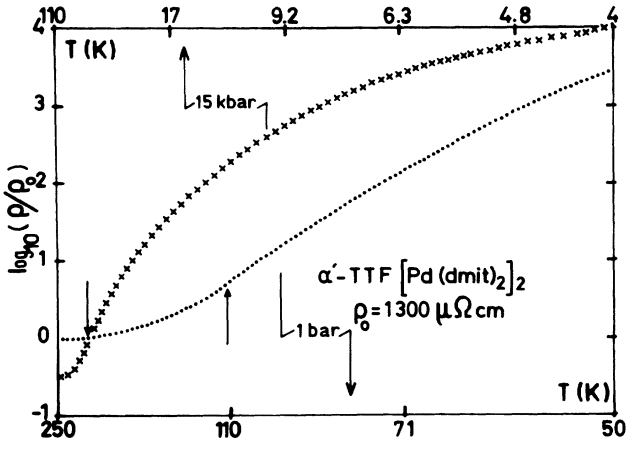

FIG. 9. log of the TTF $[Pd(dmit)_2]_2$ resistivity relative to ρ_0 (at 300 K and at ambient pressure) vs $1/T$ at ambient pressure and at 15 kbar.

(i) The first one extends from some tens or hundreds bars to 4.8 kbar. A plot of $\log_{10}(\rho/\rho_0)$ versus $1/T$ (Fig. 8) may help to define as usual a temperature T_{inf} for which $d[\log_{10}(\rho/\rho_0)]/d(1/T)$ is maximum and below which a gap is opening. Such a procedure is valid not only in the case of a single band. Indeed, in the case of the Pd salt[22] the T_{inf} value (110 K) at ambient pressure corresponds to the temperature (105 K) of condensation of the second CDW.[20] If the opening gap follows the BCS law, an activation energy Δ may be determined at temperatures lower than $T_{inf}/3$ or $T_{inf}/4$. From Fig. 8, it is clear that the resistivity does not fit such a gaplike behavior over any significant temperature interval, as observed in the case (Fig. 9) of the Pd salt.[22] Similarly, plots of $\ln(\rho/\rho_0)$ versus $(T_0/T)^n$ with $\frac{1}{4}<n<1$ (Ref. 35) for the Ni salt are not significant. The same result holds for fits to degenerate semiconducting regimes[36] of the form $\ln(\rho/\rho_0)=m\ln T+\Delta/T$.

(ii) Above 4.8 kbar, an inflexion point at T_{inf} may also be defined by using the above procedure. Since the rate of increase of the resistivity below T_{min} gradually vanishes under pressure, it becomes meaningless to assign a defined value to T_{inf} above 7 kbar. Between 4.8 and 5.75 kbar (Fig. 10), the resistivity follows an unusual law below T_{inf} and down to a temperature T_0, which is equal to 6 K at 4.8 kbar, to 2.1 K at 5.3 and 5.5 kbar, and to 3 K at 5.75 kbar, respectively. This law, which is not obeyed below 4.8 kbar and above 6 kbar, is $\rho/\rho_0=e^{-(T-T_0)/\Delta_0}$, where Δ_0 increases with pressure. While the resistivity shows an activated regime at pressures below 5 kbar, a complete superconducting transition sets up at 5.75 kbar. The interesting point to discuss is "what happens in between."

At 5.5 kbar, the resistivity shows an inflexion point at $T_0=2.1$ K, followed by a relative and flat maximum at 1.75 K, then by a relative and flat minimum at 1.15 K,

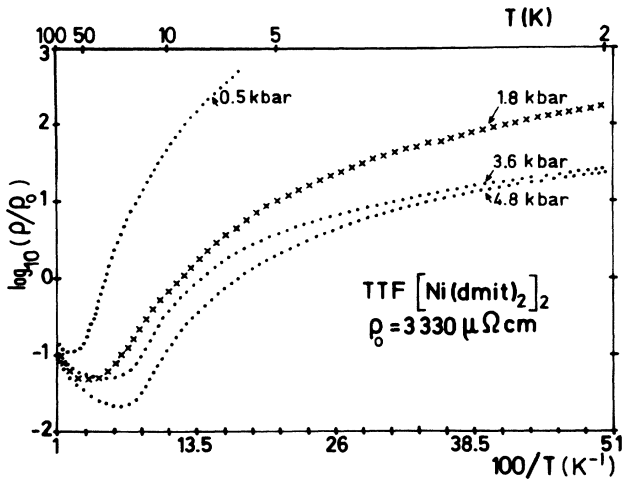

FIG. 8. log of the TTF $[Ni(dmit)_2]_2$ resistivity relative to ρ_0 (at 300 K and at ambient pressure) vs $1/T$: no exponentially activated regime is observed.

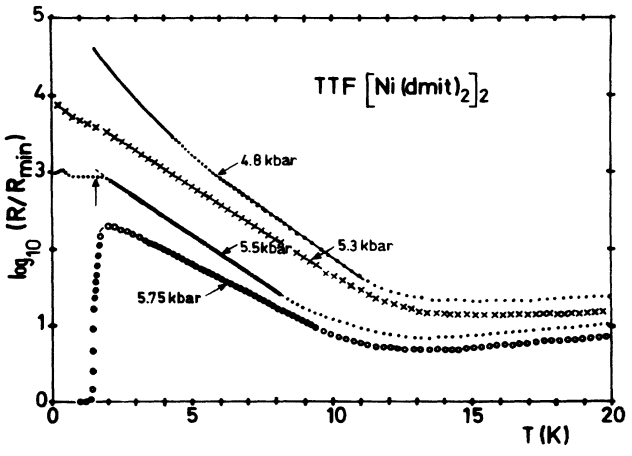

FIG. 10. log of the TTF $[Ni(dmit)_2]_2$ resistance relative to R_{min} (at 10% of the superconducting transition at 5.75 kbar) vs T; the arrow locates the temperature at which a magnetic field of 1250 G restores the normal state.

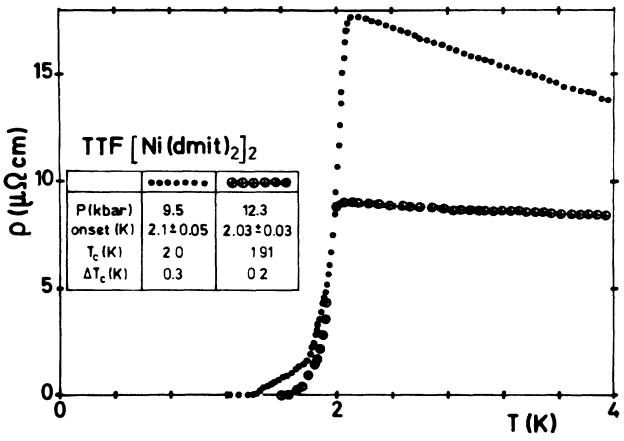

FIG. 11. Superconducting transitions of TTF $[Ni(dmit)_2]_2$ at 9.5 and 12.3 kbar.

and finally by an absolute maximum at 375 mK. At 1.54 K, a magnetic field equal to 1250 G restores the normal state, which is the signature that the sample is partly superconducting below 1.75 K. On the contrary, the increasing resistivity below 1.15 K expresses a tendency for entering the semiconducting state which prevails at lower pressure. This entrance is counterbalanced below 375 mK by the definitive reentrance into the superconducting ground state. The flatness of the relative maximum and minimum comes from inhomogeneities and/or from the nonhydrostatic character of the pressure around the sample. These factors lead to a distribution of pressures smoothing out the successive phase transitions, without altering the analysis.

At 5.3 kbar, the resistivity shows two inflexion points at $T_0=2.1$ K and at 1.4 K. No magnetic field has been applied below T_0, but two plausible explanations are suggested in order to explain the resistivity behavior: either one part of the sample becomes superconducting below T_0, while the other remains activated, or the whole sample undergoes two successive transitions into the superconducting and semiconducting ground states. The real pattern may also result from a mixture of both models.

(iii) Above 5.5 kbar, which is also the pressure above which the second small resistivity bump disappears, superconductivity sets up (Fig. 11) and its temperature T_c increases slowly with pressure: this variation is in agreement with previous low-field electron spin resonance (ESR) measurements performed on one sample.[25] The difference of 2.3 kbar between the pressure scales is similar (but not explained) with the one already observed for the Bechgaard's salt, (tetramethyltetra selenafulvalene)$_2PF_6$.[10,15] On the other hand, the shift in the superconducting temperatures results from the difference usually observed between the T_c temperatures measured either by resistivity or by radio-frequency methods.

PHASE DIAGRAM

The phase diagram of the Ni salt is shown in Fig. 12. The high- and low-temperature resistivity bumps are, respectively, represented by vertical dashed lines and dash-dotted lines; the low-temperature bump is plotted below 5.5 kbar only. The dotted curves and dash-dotted curves show the pressure dependence of the temperatures of the resistivity ρ minimum T_{min} and of the inflexion point T_{inf} of $\log_{10}\rho$ versus $1/T$; both are exponentially decreasing with pressure above ca. 4 kbar, while at first sight they seem to be dispersed at lower pressure. Above 5.3 kbar, superconductivity sets up. Its onset temperature T_c is slowly increasing (— — —) with pressure, in agreement with previous low field ESR measurements (—·—·—·).[25] At very low temperature and in a narrow pressure range around 5.3 kbar, the superconducting ground state is reentrant into the low-pressure "insulating" state. Based on simple thermodynamic grounds, this phase separation (—··—··—··) must necessarily extend somewhere towards higher temperature. The only way to achieve this extension is to consider the specific features of the temperature dependence of the resistance R reported in the Fig. 10: the linear plot of $\log_{10}(R/R_{min})$ versus T is observed (i) between 4.8 and 5.75 kbar only, and (ii) below T_{inf} and

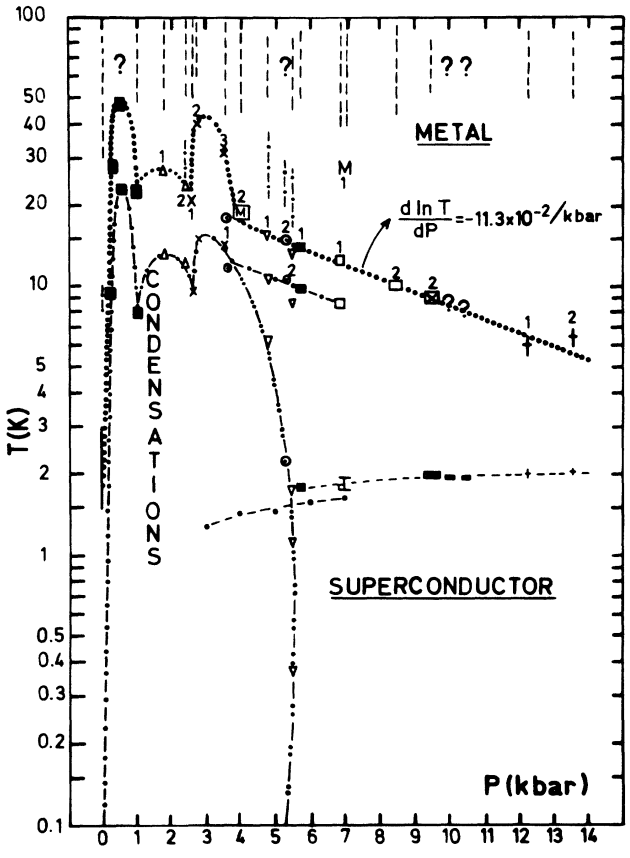

FIG. 12. Phase diagram of the TTF $[Ni(dmit)_2]_2$ compound; each sample is noted by a distinct symbol; their associated number (1, 2, or 3) indicates increasing applied pressures. Solid circles are related to measurements performed upon distinct samples. $M1$ and $M2$ refer to the sample studied in the Ref. 24; the meaning of the other symbols is detailed in the discussion (see text). Question marks mean a too high uncertainty on the measurement.

above the temperature T_0 defined in the preceding section. Although the origin of this unusual law remains unclear, the pressure dependence of T_0 may be chosen as the extension (Fig. 12) of the phase borderline ($-\cdot\cdot-\cdot\cdot-\cdot\cdot$) up to the oscillatinglike behavior of T_{inf} under pressure.

DISCUSSION

Each of the above resistivity anomalies or phase transitions is supposed connected with the three bunches of the HOMO and LUMO bands, whose signatures are the three $\mathbf{q}_i$ wave vectors of the structural instabilities observed at ambient pressure. Obviously the $\mathbf{q}_i$ values may vary under pressure, and the following hypotheses are suggested: under pressure, (i) the number of instabilities remains invariant, (ii) the $\mathbf{q}_1$ and $\mathbf{q}_3$ wave vectors remain the signatures of the high-temperature resistivity bump and of the carriers condensation below T_{inf}, respectively, and (iii) the $\mathbf{q}_2$ wave vector is connected with the low-temperature resistivity bump (below 5.5 kbar) and with the superconductivity (above 5.5 kbar). These assumptions are purely tentative and must be confirmed by diffuse x-ray measurements under pressure, but they lead to a coherent understanding of the phase diagram.

In the first 500 bars, T_{min} as well as T_{inf} increase drastically. Since the compound remains metallic down to 1.5 K at ambient pressure, these dramatic variations may be correlated with the pressure dependence of the relative band position. This induces a shift of the Fermi level, which is located between ε' and ε'' at ambient pressure (Fig. 4). Application of pressure modifies the location of the Fermi level relative to the lowest HOMO band. Any decrease of the filling of this band may first increase, then suppress the 2D hole pocket centered at the Γ point. It is suggested that the continuous increase of T_{min} and T_{inf} actually results from a continuous lessening, then suppression of the partial 2D character of the FS. This would mean that at ambient pressure the Fermi level should be located close to the intersection of the two lowest HOMO bands at the Z point, leading to a hole pocket with almost maximum area. At a given pressure, this pocket collapses when the Fermi level is located close to ε', i.e., for a high density of states concentrated around a Van-Hove–like singularity at the center of the Brillouin zone. Correlation effects may remove the degeneracy of this singularity, which could be at the origin of the oscillating character of T_{min} and T_{inf} up to 4 kbar. Above 4 kbar, since T_{min} and T_{inf} decrease continuously with pressure—as observed in the quasi-one-dimensional Pd salt—it is suggested that the Ni salt is entering the 1D regime. Hence, in opposition with most of the organic conductors, the pressure induces 1D electronic properties in this salt. A similar behavior[37] has been suggested in the organic metal (2,5-dimethyl-*N*,*N*′-dicyanoquinonediimine)$_2$Cu, but in that compound the metal-semiconductor transition should be regarded as a cooperative phenomena of the 1D electronic system formed by the organic molecules and the Jahn-Teller distortion derived from localized Cu^{2+} ions.

As already pointed out, our approach emphasizes the influence of the low-temperature correlations between carriers. These correlations could perhaps constitute the basic ingredients of the successive pressure-induced CDW's with different $\mathbf{q}_3$ nesting vectors, which has been suggested in a previous sketch.[26] Nevertheless more accurate resistivity measurements are needed, namely isothermal excursions of the phase diagram with He gas pressure, in order to discriminate between the physics shared by all samples and what is sample dependent. It is believed that the diagram will not be very different from this one: indeed after successive measurements at low temperature and at three different pressures, one sample showed an $\mathcal{R}$ equal to 310 at ambient pressure, i.e., greater than the $\mathcal{R}$ of other samples measured for the first time. This means that the apparent dispersion of the T_{min} and the T_{inf} values is not induced by thermal cyclings.

At about 5.5 kbar, i.e., the pressure at which the Ni salt recovers the conductivity of its Pd derivative at ambient pressure, superconductivity sets up at the expense of one of the two resistivity bumps which collapses at the same time. If this bump is related to the CDW instability of wave vector $\mathbf{q}_2$ (Fig. 4), then the corresponding bunch of the HOMO bands is the center of a competition between the electron-hole condensation and the electron-electron pairing, which are both governed by the electron-phonon interaction. The density of states of this bunch at the Fermi level contributes to a superconducting temperature onset of ca. 1.75 K, but this competition is probably hidden behind the antagonism between the superconductivity and the other CDW instability of wave vector $\mathbf{q}_3$ which affects the corresponding HOMO band of the acceptors. It is suggested that these different effects of the $\mathbf{q}_2$ and $\mathbf{q}_3$ CDW instabilities upon the attractive hole-hole interaction originate in the entrance of the low-pressure "insulator" state into the superconducting ground state. It is worthwhile to recall the reentrance of the superconductivity at very low temperature. The corresponding positive slope dP/dT indicates that the entropy of the superconducting ground state is lower than the entropy of the low-pressure "insulator" one. This remark confirms the existence of the reentrance and excludes any triplet superconductivity hypothesis. Otherwise a situation similar to the one described in the ^{3}He phase diagram would have been encountered. By contrast, in the Pd salt, superconductivity arises from a competition inside all the HOMO and LUMO bands of the acceptors. This leads to a superconducting temperature onset of 6.5 K at 20 kbar, at the single multicritical point in the phase diagram.[22]

With increasing pressure, T_c increases up to $\sim$2 K; a similar pressure effect has been found[38] between ambient pressure and 20 kbar in the 2D purple bronze $Li_{0.9}Mo_6O_{17}$, the superconducting temperature increasing from 1.7 to 2.5 K. In the case of the Ni salt, the origin of such an effect may come from states belonging to the "$\mathbf{q}_3$" HOMO band, since T_{min} and T_{inf} decrease with pressure. This is the signature of the low-pressure antagonism which is converted into competing instabilities spread over a large pressure range. However, since T_{inf} is not well defined above 7 kbar, the CDW instability may

not condense and probably remains in a fluctuating regime. Moreover, and in contrast with the Pd derivative, the highest-temperature resistivity bump that may be associated with the $\mathbf{q}_1$ CDW instability, survives under pressure. This indicates that this CDW condensation is not unstable against the attractive interaction established at low temperatures. Hence, the Ni salt multiband system can be characterized by a ubiquity that is absolutely unique: the simultaneity of (i) the occurrence of the superconductivity related to the "$\mathbf{q}_2$" HOMO band, (ii) its weak competition with the CDW fluctuations related to the "$\mathbf{q}_3$" HOMO band, and (iii) its coexistence with the CDW that is associated with the "$\mathbf{q}_1$" LUMO band of the Ni(dmit)$_2$ slabs.

Up to which pressure can the last two properties survive? As an example, in $NbSe_3$ the respective pressure dependences[39] of the two independent CDW condensations temperatures are $\ln(T_2/59)=-0.135P$ up to $P=4$ kbar and $\ln(T_1/145)=-\alpha P$ with $\alpha=2.0\times10^{-2}$/kbar up to 22 kbar. Similarly, between 6 and 22 kbar the pressure dependence of the superconducting temperature is $\ln(T_c/3.5)=-\alpha(P-6)$. This illustrates the same stiffening effect of the lattice on both the $\mathbf{q}_1$ CDW and superconducting instabilities between 6 and 22 kbar, i.e., in the pressure range where these instabilities are not competing. Above 22 kbar, T_c increases at the expense of the high-temperature CDW which collapses at $\sim$40 kbar. A similar stiffening effect is observed in the Pd salt phase diagram below 16 kbar and above 20 kbar.[22] It presumably exists also in the Ni salt case above 5.5 kbar between the superconductivity and the $\mathbf{q}_1$ CDW instability, whose condensation temperature does not seem to vary under pressure. However, this effect is hidden by the slow T_c increase arising from the states freed from the $\mathbf{q}_3$ CDW fluctuations.

CONCLUSION

To summarize, quite different pressure effects have been cleared up in the isoelectronic molecular TTF $[M(\text{dmit})_2]_2$ conductors, with M=Ni and Pd. In the Pd salt, the pressure induces a strong competition between the superconducting transition and the Peierls CDW instabilities, which both affect the 1D LUMO and HOMO bands of the acceptor slabs. By contrast, the Ni derivative shows a more subtle character for its ubiquitous electronic properties under pressure: successive phase transitions between (semi)metallic, semiconducting, and reentrant superconducting ground states are induced by the pressure. The dramatic irruption of a resistivity upturn in the first 500 bars as well as the unusual oscillations of the upturn temperature up to 4 kbar may be related to the critical position of the Fermi level relative to the top of the lowest one-electron HOMO band of the acceptors. Any change of location of the Fermi level may affect the respective influences of imperfect nesting and Van-Hove–like singularity until the 2D character of the zone center has been completely removed by the pressure. These effects are implemented with those of the correlations between carriers and CDW condensates at low temperature. Nevertheless these results suggest above 6–7 kbar, the simultaneous (i) coexistence of a high-temperature CDW instability and (ii) weak competition of low-temperature CDW fluctuations, with a reentrant superconducting ground state. Further measurements and theoretical improvements are obviously needed in order to elucidate such a surprising phase diagram.

ACKNOWLEDGMENTS

It is a pleasure to thank J. Friedel, P. Chaikin, P. Monceau, and J. P. Ulmet for fruitful discussions. We greatly appreciate close collaborations with E. Canadell, S. Ravy, J. P. Pouget, and J. P. Legros. We are indebted to M. Konczykowski for use of the InSb pressure gauge and its calibration. We acknowledge J. M. Mignot for communicating to us the $NbSe_3$ phase diagram prior to publication. This work has been sponsored by the Programme Interdisciplinaire de Recherches sur les Materiaux (PIRMAT) of the Centre National de la Recherche Scientifique (CNRS) under ATP supraconducteurs 89 Contract No. 89N83/0231. The Laboratoire de Physique des Solides is associé No. LA 2 du Centre National de la Recherche Scientifique (CNRS). The Laboratoire de Chimie de Coordination du CNRS is lié par conventions à l'Université Paul Sabatier et à l'Institut National Polytechnique.

[1]N. F. Mott, *Metal-Insulator Transitions* (Taylor & Francis, London, 1974).
[2]P. W. Anderson, Phys. Rev. **109**, 1492 (1958).
[3]S. K. Chan and V. Heine, J. Phys. F **3**, 795 (1973).
[4]A. W. Overhauser, Phys. Rev. **167**, 691 (1968).
[5]A. W. Overhauser, Phys. Rev. Lett. **4**, 462 (1960); W. M. Lomer, Proc. Phys. Soc. London **80**, 489 (1962).
[6]Yu. A. Bychkov, L. P. Gor'kov, and I. E. Dzyaloshinskii, Pis'ma Zh. Eksp. Teor. Fiz. **2**, 146 (1965) [JETP Lett. **2**, 92 (1965)].
[7]R. Comes, M. Lambert, H. Launois, and H. R. Zeller, Phys. Rev. B **8**, 571 (1973).
[8]J. P. Pouget, S. K. Khanna, F. Denoyer, R. Comès, A. F. Garito, and A. J. Heeger, Phys. Rev. Lett. **37**, 437 (1976); G. A. Toombs, Phys. Rep. C **40**, 182 (1978).
[9]P. M. Williams, G. S. Parry, and C. B. Scruby, Philos. Mag. **29**, 695 (1974); J. A. Wilson, F. J. Di Salvo, and S. Mahajan, Phys. Rev. Lett. **32**, 882 (1974).
[10]D. Jerome and H. Schulz, Adv. Phys. **31**, 299 (1982).
[11]T. M. Rice and G. K. Scott, Phys. Rev. Lett. **35**, 120 (1975).
[12]D. Jerome, C. Berthier, P. Molinie, and J. Rouxel, J. Phys. (Paris) Colloq. **37**, C4-125 (1976).
[13]P. Monceau, *Electronic Properties of Inorganic Quasi 1D Compounds* (Reidel, Dordrecht, 1985).
[14]J. Labbe and J. Friedel, J. Phys. Rad. **27**, 708 (1966).
[15]L. J. Azevedo, J. E. Schirber, J. M. Williams, M. A. Beno, and D. R. Stephens, Phys. Rev. B **30**, 1570 (1984).
[16]T. F. Smith, R. N. Shelton, and R. E. Schwall, J. Phys. F **5**,

1713 (1975).
[17]C. W. Chu and L. R. Testardi, Phys. Rev. Lett. **32**, 766 (1974).
[18]M. Bousseau, L. Valade, M. F. Bruniquel, P. Cassoux, M. Garbauskas, L. Interrante, and J. Kasper, Nouv. J. Chim. **8**, 3 (1984); M. Bousseau, L. Valade, J. P. Legros, P. Cassoux, M. Garbauskas, and L. Interrante, J. Am. Chem. Soc. **108**, 1908 (1986).
[19]A. Kobayashi, H. Kim, Y. Sasaki, R. Kato, and H. Kobayashi, Solid State Commun. **62**, 57 (1987).
[20]S. Ravy, J. P. Pouget, L. Valade, and J. P. Legros, Europhys. Lett. **9**, 391 (1989).
[21]E. Canadell, I. E.-I. Rachidi, S. Ravy, J. P. Pouget, L. Brossard, and J. P. Legros, J. Phys. (Paris) **50**, 2967 (1989).
[22]L. Brossard, M. Ribault, L. Valade, and P. Cassoux, J. Phys. (Paris) **50**, 1521 (1989).
[23]J. P. Ulmet, P. Auban, A. Khmou, L. Valade, and P. Cassoux, Phys. Lett. **113A**, 217 (1985).
[24]L. Brossard, M. Ribault, M. Bousseau, L. Valade, and P. Cassoux, C. R. Acad. Sci. Ser. B **302**, 205 (1986).
[25]J. E. Schirber, D. L. Overmyer, J. M. Williams, H. H. Wang, L. Valade, and P. Cassoux, Phys. Lett. A **120**, 87 (1987).
[26]L. Brossard, M. Ribault, L. Valade, and P. Cassoux, C. R. Acad. Sci. Ser. B **309**, 1117 (1989).
[27]J. P. Legros and L. Valade, Solid State Commun. **68**, 599 (1988).
[28]J. E. Schirber, Cryogenics **10**, 418 (1970).
[29]M. Konczykowski, M. Baj, E. Szafarkiewicz, L. Konczewicz, and S. Porowski, *High Pressure and Low Temperature Physics* (Plenum, New York, 1978), p. 523. Gauges are available at the High Pressure Research Center, 01-142, Warszawa, Ul. Sokolowska 29/37, Poland.
[30]W. Kang, state thesis, Université Paris—Sud, 1989.
[31]S. Ravy, E. Canadell, and J. P. Pouget, *The Physics and Chemistry of Organic Superconductors* (Springer-Verlag, Berlin, 1990), p. 252.
[32]S. Barisic, J. Phys. (Paris) Colloq. **39**, C2-32 (1978).
[33]C. Bourbonnais, P. Wzietek, D. Jerome, L. Valade, and P. Cassoux, Europhys. Lett. **6**, 177 (1988).
[34]These respective values must be corrected in Refs. 26 and 22.
[35]E. M. Hamilton, Philos. Mag. **26**, 1043 (1972); A. N. Bloch, R. B. Weisman, and C. M. Varma, Phys. Rev. Lett. **28**, 753 (1972).
[36]P. Pavlov and A. Khokhlov, *Solid State Physics* (Mir, Moskva, 1989).
[37]T. Mori, K. Imaeda, R. Kato, A. Kobayashi, H. Kobayashi, and H. Inokuchi, J. Phys. Soc. Jpn. **56**, 3429 (1987).
[38]C. Escribe Filippini, J. Beille, M. Boujida, J. Marcus, and C. Schlenker, Physica C **162-164**, 427 (1989).
[39]A. Briggs, P. Monceau, M. Nunez Regueiro, J. Peyrard, M. Ribault, and J. Richard, J. Phys. **13**, 2117 (1980); M. Nunez Regueiro, J. M. Mignot, and D. Castello (unpublished).